Microstructure evolution of zircaloy-4 during Ne ion irradiation and annealing: An *in situ* TEM investigation*

Shen Hua-Hai(申华海)[a)b)], Peng Shu-Ming(彭述明)[c)], Zhou Xiao-Song(周晓松)[c)], Sun Kai(孙 凯)[b)], Wang Lu-Ming(王鲁闽)[b)], and Zu Xiao-Tao(祖小涛)[a)†]

[a)] *School of Physical Electronics, University of Electronic Science and Technology of China, Chengdu* 610054, *China*
[b)] *Department of Materials Science and Engineering, University of Michigan, Ann Arbor, MI* 48109, *USA*
[c)] *Institute of Nuclear Physics and Chemistry, China Academy of Engineering Physics, Mianyang* 621900, *China*

(Received 26 July 2013; revised manuscript received 18 September 2013; published online 24 January 2014)

The microstructural evolution of zircaloy-4 was studied, including the amorphization and recrystallization of Zr(Fe, Cr)$_2$ precipitates, and the density of dislocations under *in situ* Ne ion irradiation and post annealing. The results show that irradiation at a relatively high temperature and dose induces the formation of nanocrystals in pre-amorphized Zr(Fe, Cr)$_2$ precipitates. The recrystallized nanocrystals also have the structure of hcp-Zr(Fe, Cr)$_2$. The formation of the nanocrystals is thought to be the consequence of competition between atomistic disordering and the recrystallization of precipitates under ion irradiation. The free energy of the nanocrystal is lower than that of the amorphous state, which is another reason for the recrystallization of the precipitates. With increased annealing temperature, the density of the nanocrystals is increased. The dislocation density sharply decreases with the increase in the annealing temperature, and its size increases.

Keywords: recrystallization, dislocation, radiation damage, zircaloy-4

PACS: 61.82.–d, 81.10.Jt, 61.43.Dq, 61.72.Ff **DOI:** 10.1088/1674-1056/23/3/036102

1. Introduction

Zirconium alloys have been extensively used in fuel-cladding and structural materials in nuclear power reactors[1–7] as they have a low absorption cross section for the thermal neutrons. To improve the performance of zircaloy in extremely hazardous environments, different zircaloys with different alloyed elements have been developed in recent decades, including ZIRLO,[8] E635,[9] M5,[2,10] Zr-4,[2,4–6] and Zr-2.[11] Both the macroscopic mechanical and the corrosion resistance properties are critical factors determining their eligibility for use in nuclear reactors.[12–14]

The macroscopic properties of materials are directly affected by their microstructures, including the void concentration,[15] dislocation loops,[10,16] and secondary phase particles (SPP).[17,18] Different kinds of SPPs have been observed in differently fabricated zircaloys. The hexagonal-closed-packed (hcp) structure of Zr(Fe, Cr)$_2$, with lattice constants of $a = 0.502$ nm and $c = 0.818$ nm, is the main precipitate in Zr-4 alloy. The Zr(Fe, Cr)$_2$ precipitation improves the corrosion resistance; however, under neutron irradiation, it is subject to amorphization.[5] The generation of dislocation loops due to neutron irradiation transforms zircaloy from ductile to brittle. Therefore, the lifetime of Zr-4 is limited by the amorphization of SPP and the formation of dislocation loops.

Crystalline–amorphous (C–A) structural transition under ion irradiation has been observed in many materials.[19–23] The basic mechanism for the C–A transition is believed to be the accumulation of many atomic displacements induced by ion or electron collisions. For U_3Si and Zr_3Al[24] consisting of 10 μm martensite laths before ion irradiation, the critical amorphization doses are 1.2×10^{18} Kr^+/m^2 (0.3 displacement per atom (dpa)) and 2.7×10^{18} Kr^+/m^2 (0.8 dpa), respectively. The critical temperatures of the C–A transition for U_3Si and Zr_3Al are 300 °C and 250 °C,[24] above which, at an irradiation temperature of 390–450 °C, the martensite laths disappear from the transmission electron microscope (TEM) image. This is accompanied by the appearance of nano grains smaller than 20 nm when the irradiation dose is lower than 2.7×10^{19} Kr^+/m^2. With an increasing irradiation dose, the amount of nanocrystals gradually increases. The phenomenon of irradiation-induced precipitation of nanocrystals is also observed in single crystals of $Ca_2La_8(SiO_4)_6O_2$, Fe_2SiO_4, and Zr_2SiO_4.[25,26] Above the critical C–A transition temperature, the irradiated materials do not amorphize, but instead of crystallization, the atomic damage cascades to produce chemical disordering and changes the free energy of the materials.

The C–A transition of Zr(Fe, Cr)$_2$ precipitates has been reported by Kai *et al.*[18] and Lefebvre *et al.*,[27] and also by Rodriguez *et al.*[28] on the basis of the metastable free-energy diagram. Yang *et al.*[5,29] demonstrated that Zr(Fe, Cr)$_2$ starts to amorphize when the neutron irradiation is up to 2 dpa at 288 °C, and dislocation loops are also observed, which alter-

*Project supported by the Key Laboratory of Neutron Physics of China Academy of Engineering Physics (Grant No. 2012AB02), the Fundamental Research Funds for the Central Universities of China (Grant No. ZYGX2012YB017), and the Major Program of the National Natural Science Foundation of China (Grant No. 91126001).

†Corresponding author. E-mail: xtzu@uestc.edu.cn

© 2014 Chinese Physical Society and IOP Publishing Ltd

natively yields the degradation of the mechanical properties. Proton irradiation has been employed to simulate the neutron irradiation-induced microstructure damage in Zr-4. The amorphization phenomenon of $Zr(Fe, Cr)_2$, accompanied by the Fe loss in the precipitation, was observed when Zr-4 was irradiated under a 2 MeV proton beam at 310 °C.[17]

We have previously reported changes in the microstructure of the irradiated Zr-4 alloy under *in situ* Ne irradiation.[17] We found that the density of the dislocation continues to increase with the increasing dose ($\sim$ 2.7 dpa), while $Zr(Fe, Cr)_2$ starts to amorphize when irradiated under a high-dose Ne irradiation at 350 °C. In the present study, we present the behavior of the alloy under a much higher-dose Ne irradiation ($\sim$ 7 dpa), and the phenomenon of recrystallization of $Zr(Fe, Cr)_2$. In addition to the change in the crystal structure of $Zr(Fe, Cr)_2$ due to Ne irradiation, *in situ* annealing of the irradiated Zr-4 alloy is studied.

2. Experimental methods

The cold-worked stress-relief-annealed (SRA) zircaloy-4 sample used in this work was provided by Western Zirconium Inc., and its composition has been reported elsewhere.[17,18,27] SRA zircaloy-4 is primarily used for pressured water reactor (PWR) cladding. The *in situ* Ne ion irradiation was conducted in a Hitachi H-9000 TEM operating at 300 keV at the IVEM/Accelerator Facility at Argonne National Laboratory. The TEM specimens were prepared by a conventional jet electrochemical polishing procedure using a solution containing 10% perchloric acid plus 90% methanol at −40 °C and a voltage of 40 V. The Ne ion with an energy of 600 keV is supposed to have a projection range of 595 nm, calculated by the stopping and range of ions in matter (SRIM) program.[30] A displacement energy of 40 eV was chosen for the SRIM calculation. It is reasonable to assume that most Ne ions have penetrated throughout the observed thin areas of the TEM specimens. Therefore, the dpa values at a depth of $\sim$ 100 nm are considered as the dpa values after the zircaloy has been Ne^+-irradiated to a certain dose as the TEM sample is about 100 nm thick. The irradiation temperature and the displacement rate were 350 °C and 10^{-3} dpa/s, respectively. The final Ne ion irradiation was ended at a dose of $\sim$ 7 dpa, followed by *in situ* heat treatment at different conditions (500 °C for 30 min, 700 °C for 10 min, and 850 °C for 10 min, as shown in Table 1) in the TEM with a temperature ramping rate of 10 °C/min.

3. Results and discussion

Figure 1(a) shows a bright-field (BF) image of a $Zr(Fe, Cr)_2$ particle with irradiation damage up to 2.7 dpa at 350 °C. The inset is the corresponding selected-area electron diffraction (SAED) pattern showing the typical amorphous halo features, from which we can conclude that the $Zr(Fe, Cr)_2$ particle has been completely amorphized by Ne irradiation.[17] The bright diffraction spots are ascribed to the Zr matrix.

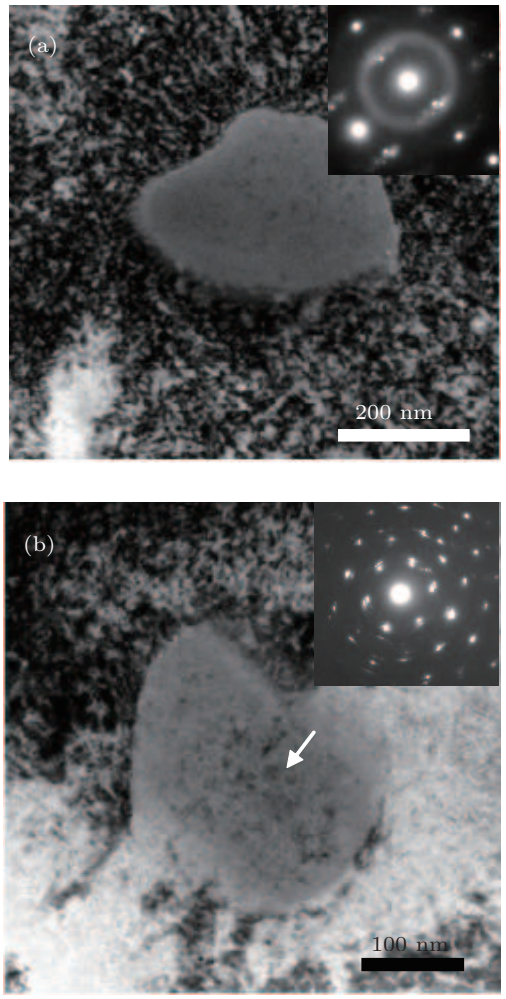


Fig. 1. Bright-field images and (inset) the corresponding SAED patterns of $Zr(Fe, Cr)_2$ particles in zircaloy-4 after *in situ* 600 keV Ne^+ irradiation up to (a) 2.7 dpa and (b) 7 dpa at 350 °C. The hcp-$Zr(Fe, Cr)_2$ spot in the SAED pattern disappears and an amorphous ring begins to appear up to 2.7 dpa, while nanoparticles start precipitating in the BF image and diffraction spots appear on the amorphous halo in the SAED pattern up to 7 dpa.

Figure 1(b) shows a BF image and the corresponding SAED pattern of a $Zr(Fe, Cr)_2$ precipitate after the Zr-4 alloy has been irradiated to 7 dpa at the same temperature. Many nanograins, with one marked by a white arrow, can be seen to decorate the $Zr(Fe, Cr)_2$ particle. The nanograins are visible with black contrast in the BF image and are almost 20 nm. The SAED pattern in the inset of Fig. 1(b), which is different from that in Fig. 1(a), shows some crystalline diffraction spots overlapping the halo. The diffraction spots overlapping the amorphous halo stem from the recrystallized nanograins. It can be concluded that the pre-amorphized $Zr(Fe, Cr)_2$ precipitate has started to recrystallize after 7 dpa Ne irradiation at the irradiation temperature. As mentioned in the introduction, irradiation can induce the amorphization of ceramics and intermetallic compounds. So the precipitation of the

$Zr(Fe, Cr)_2$ nanocrystals is also attributed to the competition between amorphization and recrystallization. One can also speculate that the recrystallization would be induced by the proposed competition mechanism during irradiation. Here, the precipitation of nanocrystals $Zr(Fe, Cr)_2$ is thought to be a consequence of the competition between amorphization and recrystallization.[24–26,31] In addition, the crystal structure of the nanocrystals remains the same as that of hcp-$Zr(Fe, Cr)_2$.

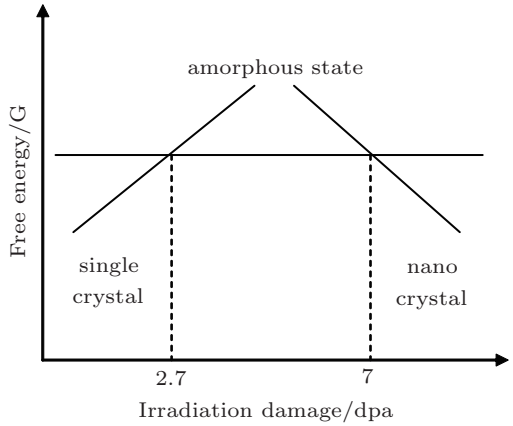


Fig. 2. Schematic diagram of the free-energy change with dpa value.

The chemical disordering and accumulation of point defects, which are produced by ion collisions, change the free energy of the $Zr(Fe, Cr)_2$ precipitate. Therefore, the variation in free energy of the system may also be a reason for the formation of the nanocrystals during irradiation. Nagase *et al.*[32] found that MeV electron irradiation can induce crystallization in metallic glasses, as a large composition fluctuation is introduced by electron irradiation. The composition fluctuation introduced by irradiation always leads to the devitrification of the amorphous phase in some metallic glasses, which has also been demonstrated by Brimhall *et al.*[33] and Doi *et al.*[34] Besides, the crystallization temperature of amorphous alloys has been found to be significantly lower if irradiated by heavy ions or electrons during annealing.[33] As for the unirradiated Zr-4 alloy, it has been proved that the $Zr(Fe, Cr)_2$ precipitate is single-crystalline.[15] After Ne ion irradiation, the increase in both the chemical disorder and the density of point defects increases the free energy of the single-crystal phase of $Zr(Fe, Cr)_2$, thus shortening the free-energy disparity between the single-crystal phase and the amorphized phase. Once the irradiation damage has reached 2.7 dpa, the free energy of the amorphous phase will be lower than that of the single-crystal phase. Thus the single-crystal $Zr(Fe, Cr)_2$ starts to amorphize. With the increase in the irradiation damage to 7 dpa, the free energy of the recrystallized nanograins is lower than that of the amorphous state due to the high thermal and composition fluctuation at a high irradiation temperature of 350 °C, thus inducing the formation of nanocrystals. This proposed mechanism is schematically shown in Fig. 2.

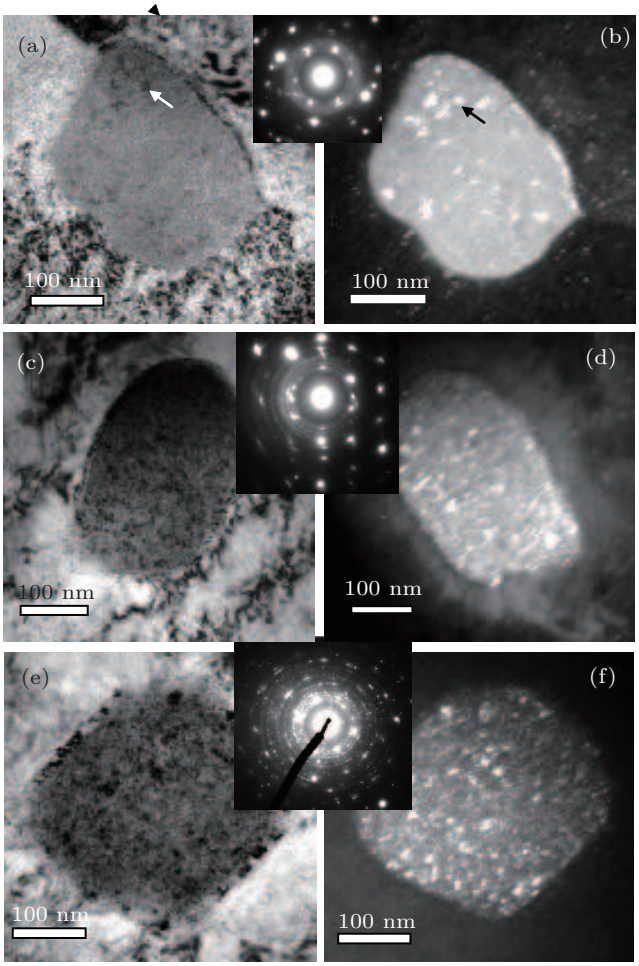


Fig. 3. The BF, DF images and (inset) the corresponding SAED patterns of the $Zr(Fe, Cr)_2$ particles, which were 600 keV Ne^+ irradiated *in situ* up to 7 dpa at 350 °C after heat annealing at 500 °C for 30 min ((a), (b)), 700 °C for 10 min ((c), (d)), and 850 °C for 10 min ((e), (f)).

Figure 3 shows the BF and dark-field (DF) images of the $Zr(Fe, Cr)_2$ precipitate after the specimen has been annealed at 500 °C for 30 min, 700 °C for 10 min, and 850 °C for 10 min. The insets in each of the images are the corresponding SAED patterns taken from the $Zr(Fe, Cr)_2$ region. Note that the diffraction spots of the Zr matrix are also present in the SAED pattern, as the size of the smallest diffraction aperture is larger than that of the $Zr(Fe, Cr)_2$ precipitate. In the $Zr(Fe, Cr)_2$ particles, many nanograins are observed, as marked by the arrows in both the BF and the DF images. From all three SAED patterns in Fig. 3, with the appearance of the obvious polycrystalline rings, we can draw a conclusion about the formation of nanocrystals in the $Zr(Fe, Cr)_2$ particles. As shown in Fig. 3(a) and 3(b), once the irradiated Zr-4 alloy has been *in situ*-heated at 500 °C for 30 min, recrystallization has started, resulting in the formation of ∼20 nm sized crystals. Obvious polycrystalline rings appear in the SAED pattern. From Fig. 3(c) and 3(d), the density of the nanograins becomes higher, while the intensity of the polycrystalline rings increases and the polycrystalline rings in the SAED patterns become sharper. This suggests that the amount of nanocrystals significantly increases after annealing at 700 °C for 10 min.

The density of the nanocrystals continues increasing with the development of the annealing. Figure 4 shows a BF image of the Zr(Fe, Cr)$_2$ precipitate and the SAED patterns of the Zr matrix and the Zr(Fe, Cr)$_2$. The Zr(Fe, Cr)$_2$ particle composed of nano-sized grains is the recrystallized Zr(Fe, Cr)$_2$, as identified by the SAED. From Fig. 4(b), we can see that the Zr matrix retains the hcp structure, with less damage by the irradiation. The polycrystalline rings appearing in Fig. 4(c) originate from the Zr(Fe, Cr)$_2$ particle indexed as the hcp structure.[35] The structure is the same as that of the precipitate before irradiation.[15]

Table 1. The dislocation density evolution of the zircaloy-4 alloy with 7 dpa pre-irradiation, induced by annealing under different conditions.

Annealing temperature/°C	Annealing time/min	Dislocation density/10^{21} m^{-3}
Pre-irradiated sample		11
500	30	9
700	10	4
850	10	0.2

Figure 5 shows BF images of the irradiated sample, showing the evolution of the dislocation density with the progress in annealing. The statistics for the approximate dislocation densities after annealing under different conditions are tabulated in Table 1. The dislocation densities decrease with an increase in the annealing temperature, starting from about 11 $\times$ 10^{21} m^{-3} before annealing to 0.2 $\times$ 10^{21} m^{-3} for the sample annealed at 850 °C. In comparison with the decrease in the dislocation densities, the dislocation lengths increase substantially with the progress of the annealing due to the migration of the point defects becoming highly activated during annealing, resulting in the aggregation of dislocations.

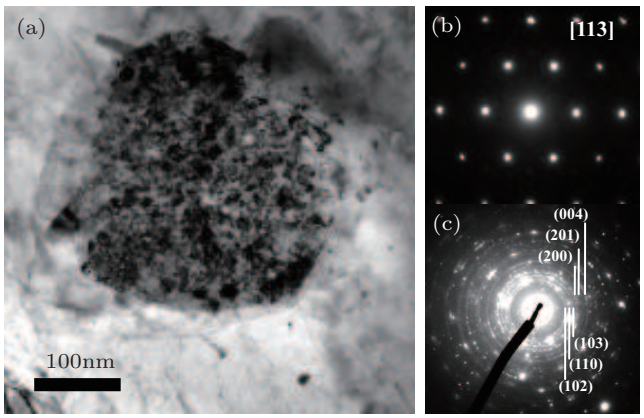


Fig. 4. The BF image (a) of the Zr(Fe, Cr)$_2$ particle after heat annealing at 850 °C for 10 min. Panels (b) and (c) show the corresponding SAED patterns of the pure-Zr matrix and precipitated Zr(Fe, Cr)$_2$ nanocrystals. After annealing, the microstructure of the matrix remains unchanged, but the SAED pattern shows significant precipitation of nanocrystals in the Zr(Fe, Cr)$_2$ particle.

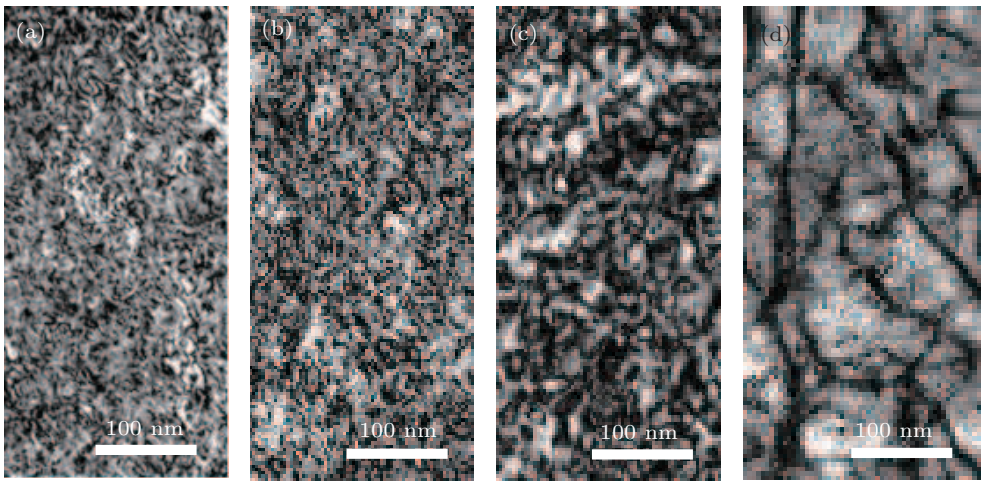


Fig. 5. The dislocation evolution of zircaloy-4, which was 600 keV Ne^+ irradiated up to 7 dpa *in situ* at 350 °C (a), due to heat annealing at (b) 500 °C for 30 min, (c) 700 °C for 10 min, and (d) 850 °C for 10 min. Before annealing, the dislocation density is about 11 $\times$ 10^{21} m^{-3}. After annealing for 30 min at 700 °C, the dislocation density becomes 9 $\times$ 10^{21} m^{-3}, and about 0.2 $\times$ 10^{21} m^{-3} after annealing for 10 min at 850 °C.

4. Conclusion

In the present study, we found the following. 1) The precipitate of Zr(Fe, Cr)$_2$ amorphizes at the Ne irradiation of 2.7 dpa at 350 °C. Then it starts to crystallize after the irradiation has reached 7 dpa at the same temperature. The large thermal and compositional fluctuations at high temperatures explain the formation of the nanocrystals. 2) A large amount of nanocrystals form in the pre-amorphized Zr(Fe, Cr)$_2$ after *in situ* heat annealing. The density of the nanocrystals increases with an increase in annealing temperature. 3) The dislocation density decreases with the increase in the annealing temperature, with the dislocation length also significantly increased.

References

[1] Négyesi M, Burda J, Bláhová O, Linhart S and Vrtílková V 2011 *J. Nucl. Mater.* **416** 288

[2] Duriez C, Dupont T, Schmet B and Enoch F 2008 *J. Nucl. Mater.* **380** 30

[3] Cockeram B V and Chan K S 2009 *J. Nucl. Mater.* **393** 387

[4] Grosse M, Berg M, Goulet C and Kaestner A 2012 *J. Phys: Conference Series* **340** 012106

[5] Yang W J S 1988 *J. Nucl. Mater.* **158** 71

[6] Hao X P, Wang B Y, Yu R S and Wei L 2007 *Acta Phys. Sin.* **56** 6543

[7] Cui Z G, Gou C J, Hou Q, Mao L and Zhou X S 2013 *Acta Phys. Sin.* **62** 156105 (in Chinese)

[8] Sabol G P 2005 *Journal of ASTM International.* **2** 12942

[9] Peletskii V E and Tereshina E V 2008 *High Temp.* **46** 363

[10] Hengstler-Eger R M, Baldo P, Beck L, Dorner J, Ertl K, Hoffmann P B, Hugenschmidt C, Kirk M A, PetryW, Pikart P and Rempel A 2012 *J. Nucl. Mater.* **423** 170

[11] Lucas G E, Surprenant M, DiMarzo J and Brown G J 1981 *J. Nucl. Mater.* **101** 78

[12] Onimus F, Béchade J L, Duguay C, Gilbon D and Pilvin P 2006 *J. Nucl. Mater.* **358** 176

[13] Oono N, Kasada R, Higuchi T, Sakamoto K, Nakatsuka M, Hasegawa A, Kondo S, Matsui H and Kimura A 2011 *J. Nucl. Mater.* **419** 366

[14] Was G S and Averback R S 2012 *Radiation Damage Using Ion Beams* (Oxford: Elsevier) pp. 195–221

[15] Boltax A, Foster J P, Weiner R A and Biancheria A 1977 *J. Nucl. Mater.* **65** 174

[16] Etienne A, Hernández-Mayoral M, Genevois C, Radiguet B and Pareige P 2010 *J. Nucl. Mater.* **400** 56

[17] Zu X T, Sun K, Atzmon M, Wang L M, You L P, Wan F R, Busby J T, Was G S and Adamson R B 2005 *Philos. Mag.* **85** 649

[18] Kai J J, Huang W I and Chou H Y 1990 *J. Nucl. Mater.* **170** 193

[19] Bloch M J 1962 *J. Nucl. Mater.* **6** 203

[20] Heera V, Stoemenos J, Kogler R and Skorupa W 1995 *J. Appl. Phys.* **77** 2999

[21] Howe L M and Rainville M H 1977 *J. Nucl. Mater.* **68** 215

[22] Quentin A, Monnet I, Gosset D, Lefranc?ois B and Bouffard S 2009 *Nucl. Instr. Meth. B* **267** 980

[23] Luzzi D E, Mori H, Fujita H and Meshii M 1985 *Scripta Metall. Mater.* **19** 897

[24] Birtcher R C and Wang L M 1991 *Nucl. Instr. Meth. B* **59–60** 966

[25] Wang L M, Wang S X, Ewing R C, Meldrum A, Birtcher R C, Newcomer P P, Weber W J and Matzke H J 2000 *Mater. Sci. Engin. A* **286** 72

[26] Wang L M and Weber W J 1999 *Philos. Mag. A* **79** 237

[27] Lefebvre F and Lemaignan C 1989 *J. Nucl. Mater.* **165** 122

[28] Rodríguez C, Tendler R H, Gallego L J and Alonso J A 1995 *J. Mater. Sci.* **30** 196

[29] Yang W J S, Tucker R P, Cheng B and Adamson R B 1986 *J. Nucl. Mater.* **138** 185

[30] Ziegler J F, Ziegler M D and Biersack J P 2010 *Nucl. Instr. Meth. B* **268** 1818

[31] Wang L M, Wang S X, Gong W L, Ewing R C and Weber W J 1998 *Mater. Sci. Engin. A* **253** 106

[32] Nagase T and Umakoshi Y 2010 *Intermetallics* **18** 1803

[33] Brimhall J L 1984 *J. Mater. Sci.* **19** 1818

[34] Doi M and Imura T 1980 *J. Mater. Sci.* **15** 2867

[35] Canet O, Latroche M, Bourée-Vigneron F and Percheron-Guégan A 1994 *J. Alloys Compd.* **210** 129